Mechanical Systems and Signal Processing 212 (2024) 111298

Contents lists available at ScienceDirect

Mechanical Systems and Signal Processing

journal homepage: www.elsevier.com/locate/ymssp

An optimal sparse sensing approach for scanning point selection and response reconstruction in full-field structural vibration testing

Jie Yuan [a,*], Michal Szydlowski [b,*], Xing Wang [c,*]

[a] Computational Engineering Design Group, University of Southampton, SO17 1BJ, Southampton, UK
[b] Dynamics Group, Imperial College London, SW7 2AZ, London, UK
[c] School of Aeronautics and Astronautics, Shenzhen Campus of Sun Yat-sen University, Shenzhen, China

ARTICLE INFO

Communicated by J.E. Mottershead

Keywords:
Compressed sensing
Fan blade
3D SLDV
Full-field vibration testing
Structural dynamics
Optimal sensor placement

ABSTRACT

Non-contact vibration measurements, such as 3D scanning laser Doppler vibrometry (3D SLDV), are becoming more prevalent in testing next-generation lightweight aerospace structures. This approach reduces the impact of attached sensors and improves measurement reliability. Acquiring precise measurement data for the whole area is feasible, albeit it would demand a considerable amount of time and storage space for testing. The concept of compressed sensing has been recently approved as an effective way to exploit signal sparsity and achieve full response reconstruction with very few measurements. The objective of this work is to enhance the efficiency of non-contact vibration testing by utilizing the state-of-the-art compressive sensing approach. In contrast to conventional sensor placement methods that rely on effective independence, modal kinetic energy, or modal assurance criterion matrix as targets, this paper proposes a novel sensor placement methodology from the perspective of dynamic response reconstruction. The scanning points are chosen with a minimal number to reduce testing time and are well-placed such that full-field vibration responses of the test structure can be reconstructed accurately. This allows for the spatially-detailed vibration responses to be obtained efficiently and accurately with optimal sparse sensing placement and effective response reconstruction through ℓ_1 algorithm. Two case studies will be presented in this work to demonstrate and validate the methodology. The first case study is focused on a simplified cantilever beam using the numerical data from the FE analysis to demonstrate the methodology. The second case study is focused on using 3D SLDV experimental testing data from a full-scale industrial fan blade. Based on the results, it is evident that the proposed approach can significantly decrease the scanning points required for a full-field dynamic response reconstruction during full-field vibration testing.

1. Introduction

Vibration can be induced from many different excitation sources, including unsteady aerodynamics flow, translating and rotating elements, imbalances from bearing, interactions and frictional contacts. The vibration properties, such as natural frequency and mode shapes, always depend on the structural properties, geometry and boundary conditions, which may also change with time due to control inputs and structure ageing, such as erosion and wear. The increasing use of large and lightweight structures also makes the dynamic properties more complicated. To ensure the reliability and durability of these structures, their complicated

* Corresponding authors.
E-mail addresses: j.yuan@soton.ac.uk (J. Yuan), michal@szydlowski.info (M. Szydlowski), wangxing5@mail.sysu.edu.cn (X. Wang).

https://doi.org/10.1016/j.ymssp.2024.111298
Received 11 October 2023; Received in revised form 16 December 2023; Accepted 26 February 2024

vibration properties have to be well understood at the design stage through a large number of vibration tests before being deployed in engineering applications. On the other hand, the results of vibration testing can be used to monitor structural integrity, allowing for robust, efficient and straightforward implementation of structural health monitoring systems [1].

Vibration testing can be conducted in two major ways: (i) where the structure is subject to real or simulated conditions in order to determine the levels of vibration response expected in service or to check if the structure does not fail; (ii) where both response and excitation signals are measured in order to understand the dynamics of the tested structure. Measuring the excitation forces and relating them to the responses allows one to build a mathematical model of the structure - a modal model [2]. Accelerometers have been one of the most widely used sensors for vibration testing. These sensors are designed to output a voltage signal proportional to the acceleration that the transducer is attached to. Since the sensors need to be attached to the structure, they may influence the response of the structure either by mass loading or damping generated by the wires that connect them to the acquisition system [3]. Laser Doppler Vibrometer (LDV) was proposed as a non-contact approach to remove the need to modify the structure and has no impact on the dynamics of the test structure. It is particularly important for modern aerospace structures made of lightweight material whose dynamics are very sensitive to additional mass-loading or damping of the measurement system. LDV is based on the Doppler frequency shift effect that occurs when light (laser beam) is scatted by a moving surface. The shift in phase is proportional to velocity, enabling contactless measurements of out-of-plane velocities of the vibrating structure [4]. The use of a pair of galvanized mirrors to relocate the laser beam enabled automated point-b-point scanning of entire structures. This technique is called scanning laser Doppler vibrometry (SLDV), which allows full-field operational deflection measurements of a structure. Although accurate, it would take a large amount of acquisition time if a large number of scan points and a fine frequency resolution were used.

For either contact or non-contact approach, the number of measured points in a vibration test is usually far fewer than the degrees of freedom of the test structure due to cost and technology constraints, which is often referred to as spatial incomplete measurement [5–7]. To further reduce the number of sensors or measurement points for improved efficiency, one of the main challenges for engineers is how to place a set with a minimum number of sensor locations where the maximum structural response information can be gained. This is known as optimal sensor placement (OSP), which is particularly important for lightweight and complicated aerospace structures such as composite wings and fan blades. These structures usually have very high modal densities and complex modal coupling [8].OSP involves two aspects: evaluation criteria for given sensor configurations and optimization method to produce an optimum choice. To evaluate sensor configurations, Kammer [9] proposed the effective independence method to maximize the determinant of the Fisher information matrix, such that the measured points contain sufficient information on targeted modal responses. From the viewpoint of improving signal-to-noise ratios of sensors, the modal kinetic method (MKE) was investigated as a criterion to ensure the maximization of the measured kinetic mode energy [10]. Targeting at mode shapes obtained from sensors, the off-diagonal element of the modal assurance criterion (MAC) matrix can also be used as a criterion to evaluate the effectiveness of the obtained mode shapes and minimize the number of sensors [11]. Other evaluation criteria, such as information entry and driving-point residue [12], have also been investigated for the purpose of sensor placement. The suitability and the performance of different evaluation criteria are also comparatively investigated in many cases. Li [13] showed that the effective independence method is an iterated version of the MKE with re-orthonormalized mode shapes. Ref. [14] compared the suitability of the Guyan reduction method and the effective independence method for sensor placement using many evaluation criteria and showed the advantages and disadvantages by using simple numerical examples. As can be seen, the aforementioned evaluation criteria rely on a finite-element model of the structure, which is not always available or accurate for realistic structures. The optimization method also plays an important role in achieving efficient OSP. Many popular algorithms such as the genetic algorithm, the particle swarm algorithm, and the ant colony algorithm [12] have been employed to solve the sensor placement problem. Recently, more advanced algorithms such as machine learning have also been attempted to reduce the computational cost for OSP [15,16] . The response time-series construction, however, has not been taken into account for OSP. It offers a new perspective to formulate the criterion that the data obtained from sensors should be able to accurately reconstruct the full-field response of the structure in space and in time [17]. The other similar sensing placement challenge is related to vibration-based structural health monitoring which requires to store and deal with a huge amount of vibration data. In particular, the case of structural health monitoring using dense sensor networks usually requires super long time sampling and produces a huge amount of data that needs to be compressed. It also promotes research on more efficient sensing methods. In the temporal domain, for example, Yang [18] proposed a principled (truncated) independent component analysis (PICA) method to compress noisy data and achieved a dramatically higher compression ratio (CR) than the wavelet method. In the spatial domain, Ganesan et al. [19] showed computational sensing can be effectively used to reduce both the volume of data and the number of sensors in vibration monitoring applications. Bhowmick and Nagarajaiah [20] presented a novel spatiotemporal compressed sensing technique for video-based measurement data where no prior assumptions of the structural properties are required. Such compressive sensing techniques can be applied to spatially-detailed vibration responses in non-contact vibration testing, which has not been investigated yet. This study is focused on reducing the non-contact vibration measurement of critical aerospace components using sparse sensing approaches.

Signals captured during structural dynamic testing exhibit, like many other natural signals, an inherent structure that enables sparse representation in a different coordinate system. The Fourier transform is an example of an operation that enables a sparse representation of a time domain signal in a new coordinate system — the frequency domain, where a small number of modes have coefficients that are significant (considered non-zero). The signal after the transformation can be truncated in such a way that only the coefficients that contribute to the signal are kept, while the others are assumed to be trivial. The truncated signal, transformed back to the time domain using the inverse Fourier transform, will retain the most significant information in the signal. Naturally, there are many more ways to express a signal in such a coordinate space where the signal is sparse. One can use the Wavelet transform, Cosine Transform, all of which consist of modes or base functions [21]. The essence of compressed sensing is to recover

a sparse signal from linear measurements using convex optimization [22]. From yet another standpoint, one can treat the problem as computing a sparse coefficient vector for a signal with respect to an over-complete system. Similarly, in the spatial domain, the number of sensors can also be reduced through sparse representation. However, it has not been much explored, especially for the recent full-field contactless modal testing of complex structures.

The objective of this paper is to efficiently and accurately obtain spatially-detailed vibration responses for industrial-scale structures using 3D scanning laser doppler vibrometry (3D SLDV). The main contribution is proposing a novel sensor placement methodology from the perspective of dynamic response reconstruction. In the method, compressive sensing techniques are used to select a minimum number of scanning points to reduce testing time before re-constructing full-field responses with prescribed accuracy. The paper is organized as follows. The theory of the sparse sensing approach will be first given. Then, the methodology will be applied to sensor optimization using two case studies showing the capability of capturing the mode shapes and reconstructing the frequency response. The first case study is focused on a cantilever beam from the numerical data. The second case study is focused on full-scale industrial fan blade testing based on 3D SLDV experimental data. For both case studies, the random sampling technique is used as a reference. The sensitivity of performance to the number of sensors will also be studied and discussed in detail.

2. Compressed sensing and sensor placement

In this section, the general principle and formulation of compressed sensing and response construction will be first introduced. It is followed by the description of the sensor placement using QR factorization.

2.1. Theory of compressed sensing

Generally a compressible response vector $\mathbf{x} \in \mathbb{R}^n$ can be expressed using a transform basis $\mathbf{\Psi} \in \mathbb{R}^{n\times n}$ as sparse vector $\mathbf{s} \in \mathbb{R}^N$ in the following way [23]:

$$\mathbf{x} = \mathbf{\Psi}\mathbf{s} \tag{1}$$

The coefficient vector $\mathbf{s} = \{s_0, s_1, \dots, s_k\}, k \ll n$ is considered k sparse in $\mathbf{\Psi}$ when the number of nonzero coefficients $K = \|\mathbf{s}\|_0$ is significantly smaller than the number of available coefficients N to reconstruct the original response $\mathbf{x}$, where $\| * \|_0$ denotes the ℓ_0 norm.

The idea of compressed sensing is to exploit the fact that the dynamical response/signal is sparse, and instead of measuring $\mathbf{x}$ directly and then compressing, it intends to achieve the full signal reconstruction from surprisingly few measurements. Given a signal $\mathbf{x}$ that is $\mathbf{K}$ sparse in $\mathbf{\Psi}$, it generally relies on special sampling techniques and reconstructing the full signal using a known basis function [24,25]. The measurement vector $\mathbf{y} \in \mathbb{R}^p$, with $p \ll n$ can be expressed by:

$$\mathbf{y} = \mathbf{C}\mathbf{x} \tag{2}$$

where $\mathbf{C}$ is the measurement matrix that represents a set of p linear measurements in the state of $\mathbf{x}$. The $\mathbf{C}$ is of critical importance in compressed sensing that may consist of random projections of the state based on Gaussian or Bernoulli distribution. With the measurement matrix, the nonzero elements $\mathbf{s}$ of the transformed coordinate system can be estimated by solving the following equation:

$$\mathbf{y} = \mathbf{C}\mathbf{\Psi}\mathbf{s} = \mathbf{\Theta}\mathbf{s} \tag{3}$$

This system equation is commonly under-determined, and there are many consistent solutions of $\mathbf{s}$. The idea of compressed sensing is to find the sparest vector $\hat{\mathbf{s}}$ that is consistent with measurements $\mathbf{y}$, which is possible to be used for the reconstruction of the full signal $\mathbf{x}$. As shown in the following equation, $\hat{\mathbf{s}}$ can be found by satisfying the following optimization problem:

$$\hat{\mathbf{s}} = \arg\min_s \|\mathbf{s}\|_0 \text{ subject to } \mathbf{y} = \mathbf{\Theta}\mathbf{s} \tag{4}$$

Generally speaking, ℓ_0 norm is not suitable for minimization because it commonly requires a direct and brutal search approach employing a combinatorial algorithm between n and K. Such an optimization process using ℓ_0 is intractable for even moderately large n and K. The other way of calculating the nonzero coefficients is by reformulating Eq. (4) in terms of ℓ_1 instead of ℓ_0 norm. The ℓ_1 norm is also known as the taxicab or Manhattan norm because it represents the distance a taxi would take between two points on a rectangular grid. This is commonly called basis pursuit and can be expressed in the following form:

$$\hat{\mathbf{s}} = \arg\min_s \|\mathbf{s}\|_1 \text{ subject to } \mathbf{y} = \mathbf{\Theta}\mathbf{s} \tag{5}$$

where $\| * \|_1$ denotes the ℓ_1 norm. This ℓ_1 norm has a few important consequences, firstly the problem is no longer NP-hard, secondly, it is no longer discontinuous and non-convex and therefore enables the use of many more optimization techniques. ℓ_2 can also be used, which usually searches a solution from a circle to minimize the least square errors. Although efficient, ℓ_2 does not much promote sparsity.

The above-mentioned problem in Eq. (5) can also be solved with methods from the regression family, with the least absolute selection and shrinkage operator (LASSO) [26] being the most popular. LASSO is a quadratic programming problem where the $\mathbf{s}$

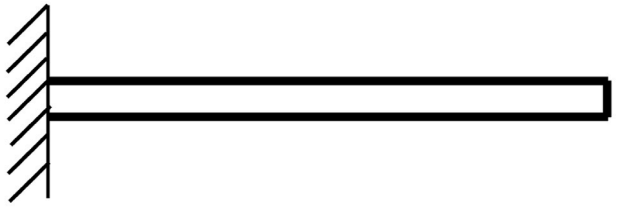

(a)

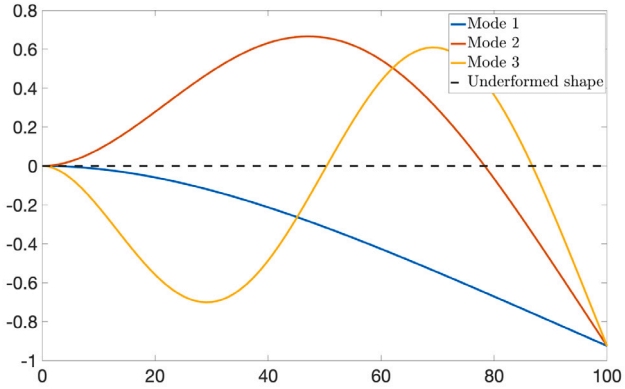

(b)

Fig. 1. (a) A cantilever beam (b) The first three mode shape.

is minimized in respect of the squared error of the sparse vector's projection onto the measurement matrix and with λ being a regularization term of the $\|\mathbf{s}\|_1$ condition that is responsible for promoting sparsity. Mathematically this can be formulated as:

$$\hat{\mathbf{s}} = \arg\min_{s} \|\mathbf{y} - \boldsymbol{\Theta}\mathbf{s}\|_2^2 + \lambda\|\mathbf{s}\|_1 \tag{6}$$

.

Alternatively, there exists a class of algorithms that allow minimization of the number of coefficients K [23,27]. To estimate the positions of the nonzero coefficient, the matching pursuit (MP) method can be used [23,27,28]. This is a greedy algorithm where the iterative projections of the measurements y onto the dictionary of basis functions are used to find the positions and values of the non-zero coefficients. Although ℓ_1 is well known for the promotion of the sparsity, ℓ_2 penalty formulation is still widely used in the modelling updating and optimization framework. The ℓ_2 norm is strictly convex and therefore by means of convex optimization results in a unique minimizer. In the case of ℓ_1 norm is not strictly convex, hence the minimizer is non unique. Additionally ℓ_1 is not strictly differentiable this results in the need for sub-gradient or proximal methods that are computationally more expensive [29]. In this study, ℓ_1 and ℓ_2 penalty formulation will be used for response reconstruction to demonstrate the effectiveness of ℓ_1 algorithm.

2.2. Optimal sparse sensor placement

As discussed previously, the sensor placement of **C** is of critical importance in compressed sensing. Optimizing sensor locations is important for nearly all downstream tasks, including classification, prediction, estimation, modelling, and control. However, identifying optimal locations involves a brute-force search through the combinatorial choices of p sensors out of n possible locations in space. The main criteria of sparse sensor placement are to design **C** in order to minimize the condition number of Θ so that it may be inverted to identify the low-rank coefficients of a given noisy measurement y. The condition number of a matrix Θ is the ratio of its maximum and minimum singular values, indicating how sensitive matrix multiplication or inversion is to errors in the input. Random sensor has been widely used in the compressive sensing for the sparse sampling in time domain, which will be used a reference in the paper.

In this study, the modal shape function of the structure will be used for the transform basis Θ. QR factorization will be used for sensor selection. It was explored by Drmac and Gugercin for reduced-order modelling, providing a particularly simple and effective sensor optimization. The QR pivoting method is fast, simple to implement, and provides nearly optimal sensors tailored to a specific SVD/POD basis. The reduced matrix QR factorization with column pivoting decomposes a matrix $A \in R^{m\times n}$ into a unitary matrix Q, an upper-triangular matrix R and a column permutation matrix C^T such that $AC^T = QR$. The pivoting procedure provides an

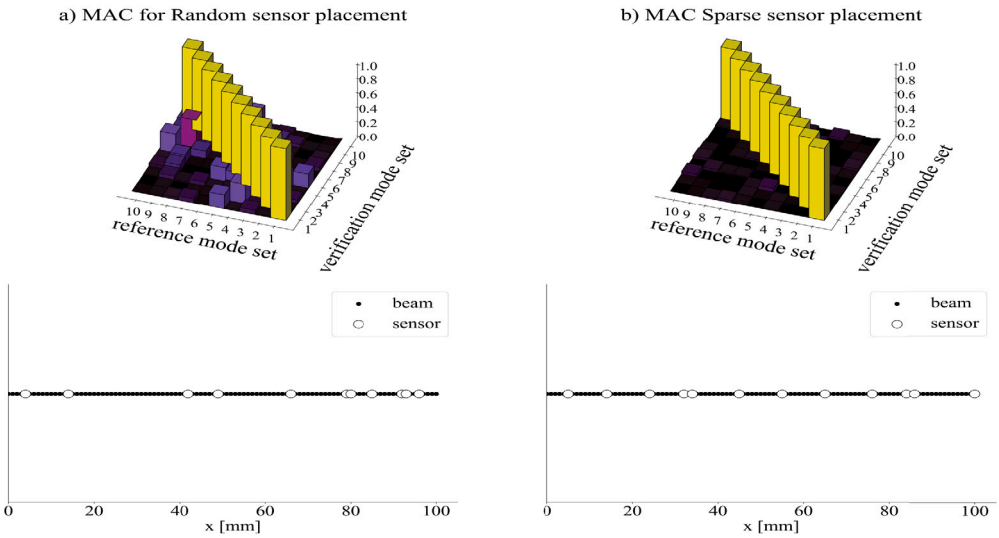

Fig. 2. Auto Mac comparison with 10 sensors.

approximate greedy solution method to minimize the matrix volume, which is the absolute value of the determinant. QR column pivoting increments the volume of the submatrix constructed from the pivoted columns by selecting a new pivot column with maximal 2-norm, then subtracting from every other column its orthogonal projection onto the pivot column.

Thus QR factorization with column pivoting yields r-point sensors (pivots) that best sample the r basis modes $\boldsymbol{\Psi}_r$,

$$\boldsymbol{\Psi}_r{}^T \mathbf{C}^T = \mathbf{QR} \tag{7}$$

Based on the same principle of pivoted QR, which controls the condition number by minimizing the matrix volume, the oversampled case (when $p > r$) is handled by the pivoted QR factorization of $\boldsymbol{\Psi}_r \boldsymbol{\Psi}_r{}^T$,

$$(\boldsymbol{\Psi}_r \boldsymbol{\Psi}_r{}^T)\, \mathbf{C}^T = \mathbf{QR} \tag{8}$$

In this study, the optimized sparse sensors will be obtained on a tailored basis with QR pivots on a universal basis using compressed sensing, which will be referred as "optimal sparse sensor" in the following text. Previous studies have shown that the performance of QR pivots with a tailored basis is much better than the random sensors from a universal basis. Furthermore, many fewer QR sensors are required for the same reconstruction performance, decreasing the cost associated with instruction and maintaining sensors. It will be further investigated in the following two studies in the context of non-contact vibration testing.

3. Numerical example: a cantilever beam

In this section, optimal sparse sensing approaches will be applied for response reconstruction for the dynamical response of a cantilever beam model. The random sensing approach is used as a reference for the study.

4. Cantilever beam model

A vibrating cantilever beam is considered a numerical example to validate the methodology of compressed sensing for the dynamical response construction. Fig. 1(a) shows a simple cantilever beam with a length of 100 mm, and the width and height of the cross-section are 25 mm and 6 mm, respectively. The beam is modelled by using the Euler–Bernoulli beam element, where each node has 2 Degrees of Freedom (DOFs) (uy,rz). The beams are made of steel with a nominal density of 7850 kg/m^3 and Young's modulus of $2.1\times10^{11}\,N/m^2$. The total number of nodes for the finite element beam is 51. Fig. 1(b) shows the first three bending modes of the beam, namely the first, second and third bending modes, where the dashed line is the undeformed shape of the cantilever beam.

4.1. Auto MAC and response reconstruction

Fig. 2 shows the comparison of the performance of these two sampling techniques: one is with random sensor placement, and the other one is with optimal sparse sensor placement. QR factorization with column pivoting based on the obtained first ten-mode shapes is used to select the sparse sensors. The two figures at the bottom show the position of 10 sensors on the cantilever beam, while the figure at the top shows the auto MAC value for each sampling method. Auto MAC is used as a criterion to evaluate the

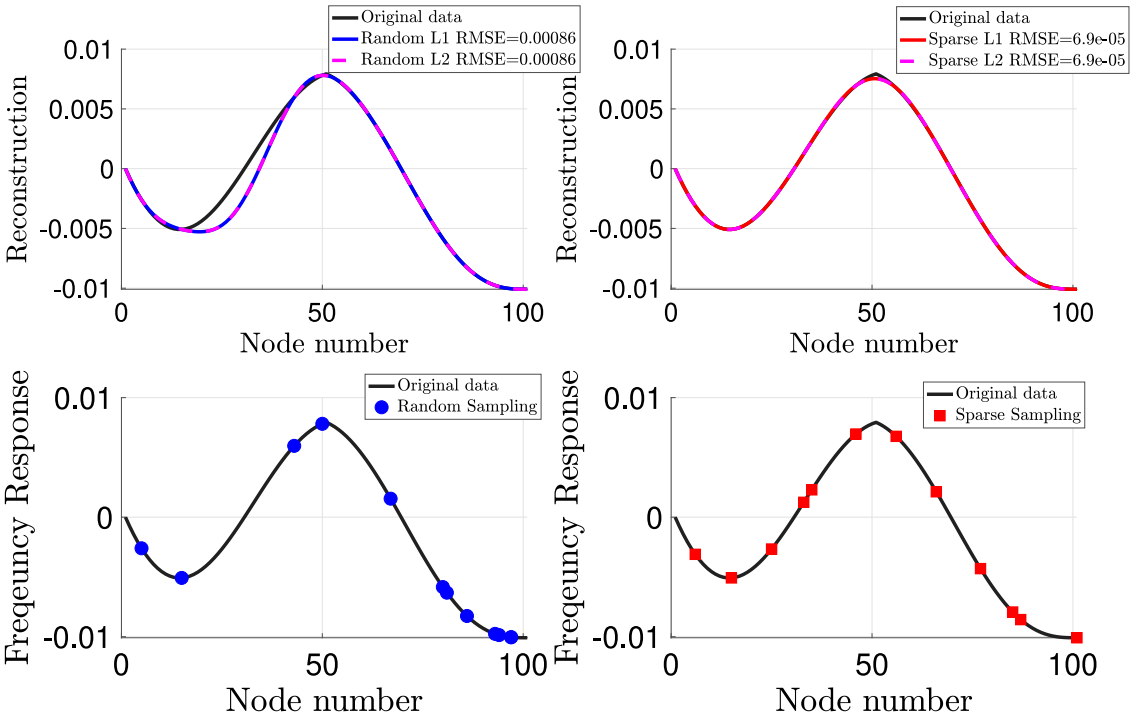

Fig. 3. ℓ_1 and ℓ_2 reconstruction of a forced response.

performance of these two types of sensor placement. It shows the distinctiveness of the mode shapes, indicating the effectiveness of the two sensor placement approaches. The auto MAC is evaluated as follows:

$$MAC_{ij} = \frac{(\boldsymbol{\Phi}_i^T \boldsymbol{\Phi}_j)^2}{(\boldsymbol{\Phi}_i^T \boldsymbol{\Phi}_i)(\boldsymbol{\Phi}_j^T \boldsymbol{\Phi}_j)} \tag{9}$$

where $\boldsymbol{\Phi}_i$ and $\boldsymbol{\Phi}_j$ are ith and jth modal vectors respectively. The off-diagonal elements of MAC matrix should be minimized so that the modal matrix measured can keep better orthogonality, which indicates a better sensor placement. One can clearly see that the optimal sparse sensor placement obtains much lower off-diagonal values with the same number of sensors. It means the mode shape sampled by the sparse sensor is more distinctive than the one sampled by the random sensor approach. Compared to Fig. 1(b), one can find that the optimal sparse sensor can effectively capture points where mode shapes have the most significant difference.

Fig. 3 shows forced frequency response construction using these two sampling approaches at a frequency of 1700 rad/s. In this case, we applied the harmonic excitation at the tip of the cantilever beam. The two figures at the bottom show the position of ten sensors using two sampling approaches. The solid black line represents the real forced frequency response. For response reconstruction, both ℓ_1 and ℓ_2 algorithms are used based on the data obtained from the sensor positions. From the top two figures, we can find there is no observable difference in response constructed using ℓ_1 and ℓ_2 algorithms. However, it shows that the response constructed from the random sampling approach has some clear differences at the node number between 20 and 40 due to the lack of sensors in this area. On the other hand, the response constructed using the sparse approach shows good agreement with the original response with a much lower RMSE value ($6.9e^{-5}$) compared to that from the random sensor (0.00086).

4.2. Sensitivity analysis

Fig. 4 shows the sensitivity of different numbers of sensors on the accuracy of response construction (RMSE L1 value) and distinctiveness of the mode shapes (Max off-diagonal Auto MAC value). The red circle represents the results from the random sampling approach, where we have used 50 Monte Carlo simulations. The blue square represents the results from the optimal sparse sensing approach based on QR factorization. It shows that the results converged when the number of sensors approached 10. With further increase of sensor number, the improvement of RMSE and off-diagonal Mac value are very limited. Compared to the random sensing approach, it shows that when the number of sensors is insufficient, such as 4, 6 and 8, some sensor placements based on the random sampling approach could have a good performance in terms of response reconstruction. The optimal sparse sensing approach can achieve more robust performance when the number of sensors is sufficient (over 10). In terms of Auto MAC value, the optimal sparse sensing approach shows a lower max off-diagonal value than any Monte Carlos simulation using the random sensor approach when the number of sensors is over 4. Fig. 5 shows the sparsity of the sparse coefficients using random sensor and

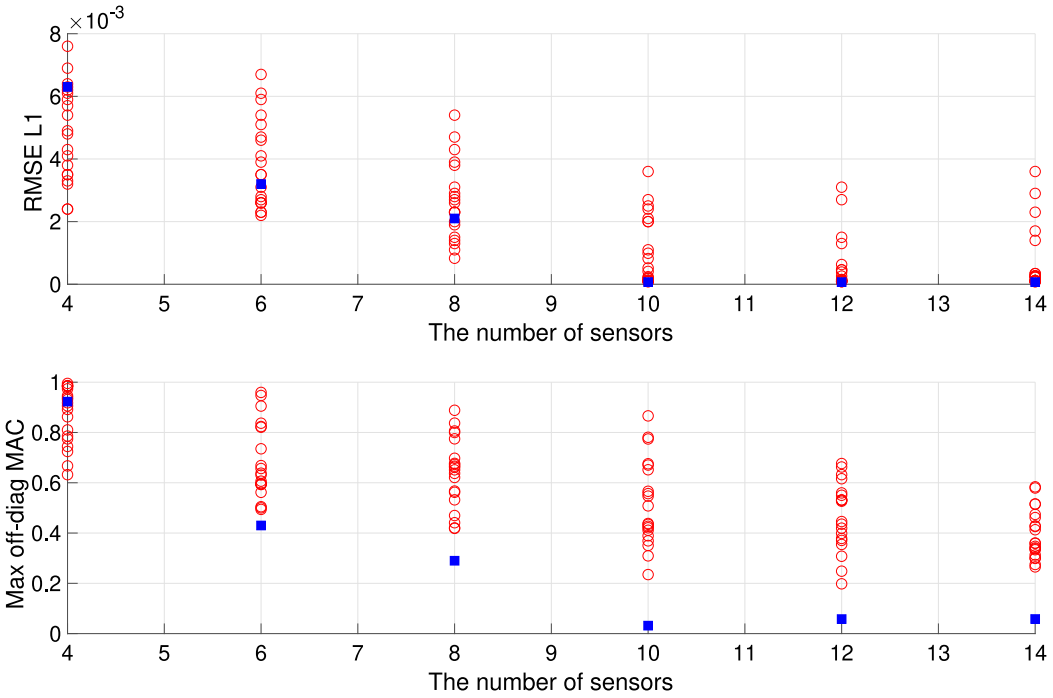

Fig. 4. Sensitivity analysis of beam with different sensors.

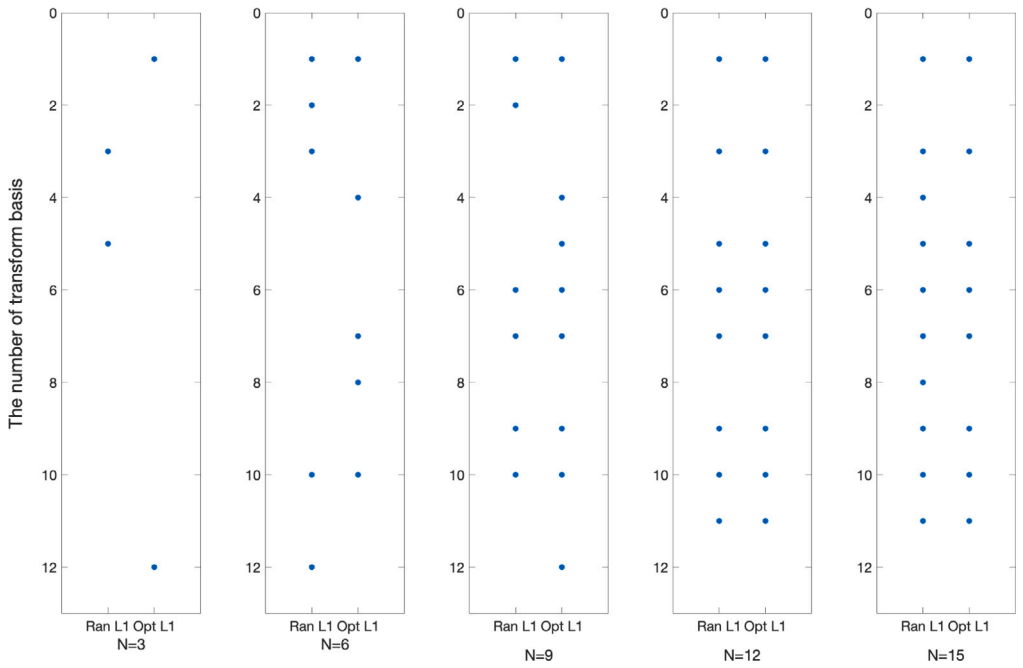

Fig. 5. Comparison of the sparsity of random sensor and optimal sensor approach for 2D beam case.

optimal sensor from ℓ_1 algorithm. With the increase in the number of sensors, the sparsity of these two approaches is very similar especially at a high number of sensors. The random sensor shows a bit more sparsity at a low number of sensors.

Fig. 6 shows the sensitivity of different levels of noise on the accuracy of response construction between the random sensing and optimal sensing approach using ℓ_1 algorithm. The level of noise is introduced to the measurement data from the sensing locations at 0.5%, 1.0%, 5.0% and 8.0%. This comparison study is carried out using 10 sensors and 12 transform bases. The results show

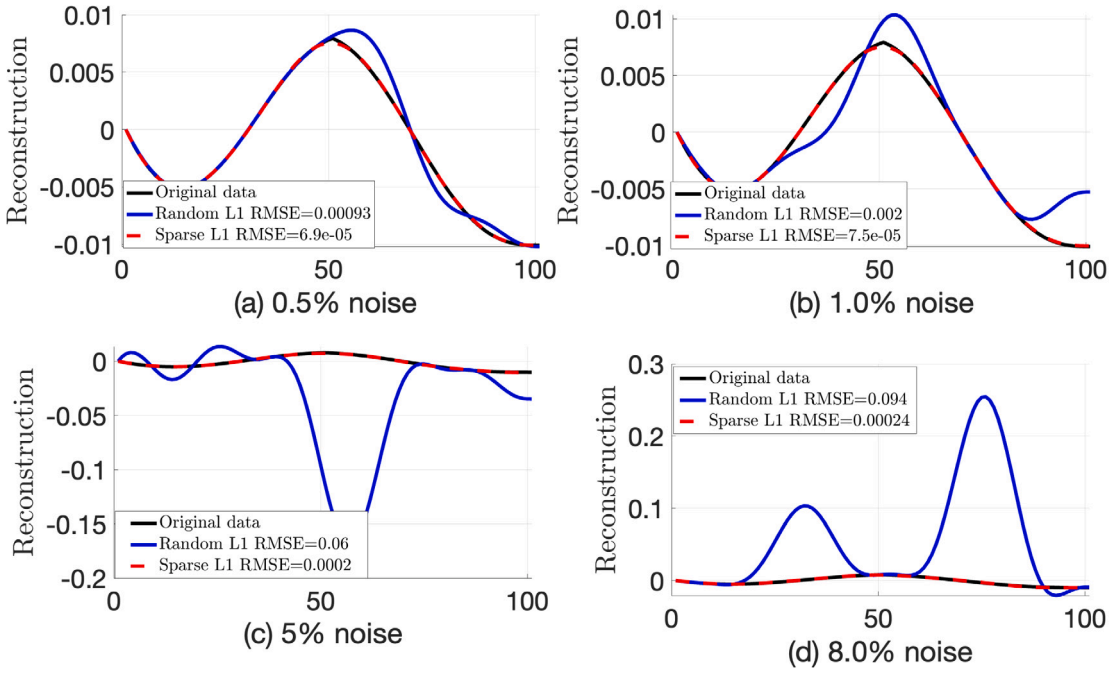

Fig. 6. Comparison of the response between random and optimal sparse sensors at different measurement noise levels.

that the RMSE of random sensing increases significantly with noise level from 0.09% to 9.4%. The response construction could not capture the original data at 5.0% and 8.0%. For optimal sensing, it is very robust to the noise level at different levels which can keep the error less than 0.024%. At the noise level of 8.0%, the reconstructed response can still capture the original data very well.

Fig. 7 shows the RMSE chartbox related to optimal sparse sensors using ℓ_1 algorithm at different levels of noise up to 10%. The box indicates the median, the lower and upper quartiles of the error, while the outliers show their minimum and maximum values. Since the noise is introduced randomly, 20 simulations are performed to obtain the statistics. As expected, it shows that the mean RMSE slowly increases with the noise level from 0.8e−4 (0% noise level) to 3e−4 (10% noise level), which should keep high accuracy of the response reconstruction as shown in Fig. 6. The confidence interval also increases with the noise level but still keeps a reasonable range even at the noise level of 10%. This sensitivity shows the great robustness of the optimal sensor approach, even under extremely noisy measurements.

5. Experimental example: a full-scale aero-engine fan blade

In this section, the proposed optimal sensor placement technique is applied to test data of a realistic fan blade. The target is to reconstruct the full-field, resonant operating deflection shapes (ODS) of the blade by using a minimal number of measured points.

5.1. Test set-up

As shown in Fig. 8(a), the blade was clamped at the root using an appropriate mechanism. A Data Physics Signal Force V4 shaker was used to apply excitation force to the blade, and the force was measured by a PCB 208C02 force transducer, as shown in Fig. 8(b). A Polytec PSV-500-3D-HV Scanning Laser Vibrometer was used to perform full-field measurement [30], and a total of 2016 scanning points were defined on the surface of the blade. Figs. 9(a) and 9(b) show the measurement grid and the coordinate system. To perform experimental modal analysis (EMA) for the fan blade, the single-shot mode of 3D SLDV was first used to measure frequency response functions (FRFs) of three representative points near the tip of the blade [30]. Next, the natural frequencies of the blade were then identified from the measured FRFs using the Least-squares rational function estimation method [31]. Using these identified natural frequencies, the vibration of the blade was tuned to resonant conditions sequentially by using a pure sinusoidal voltage with a frequency equal to an identified natural frequency of the structure. The full-field, resonant ODS of the blade was then measured by using the Fast-Scan mode of 3D SLDV, which would take approx. 3–5 min for each ODS.

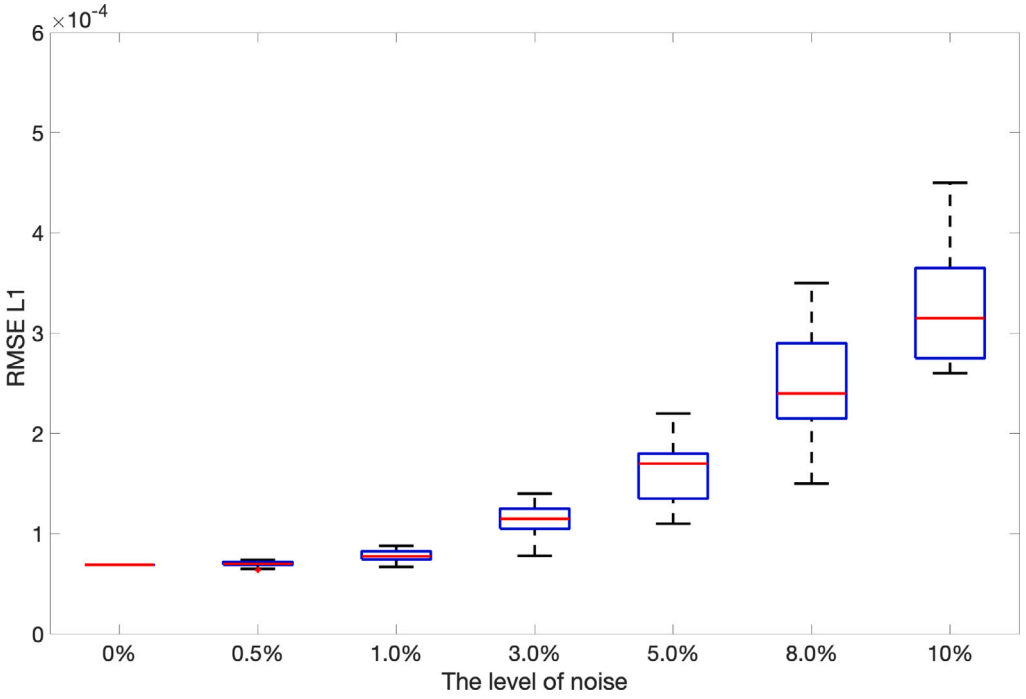

Fig. 7. Sensitivity analysis of beam with different noise levels using spare sensing approach.

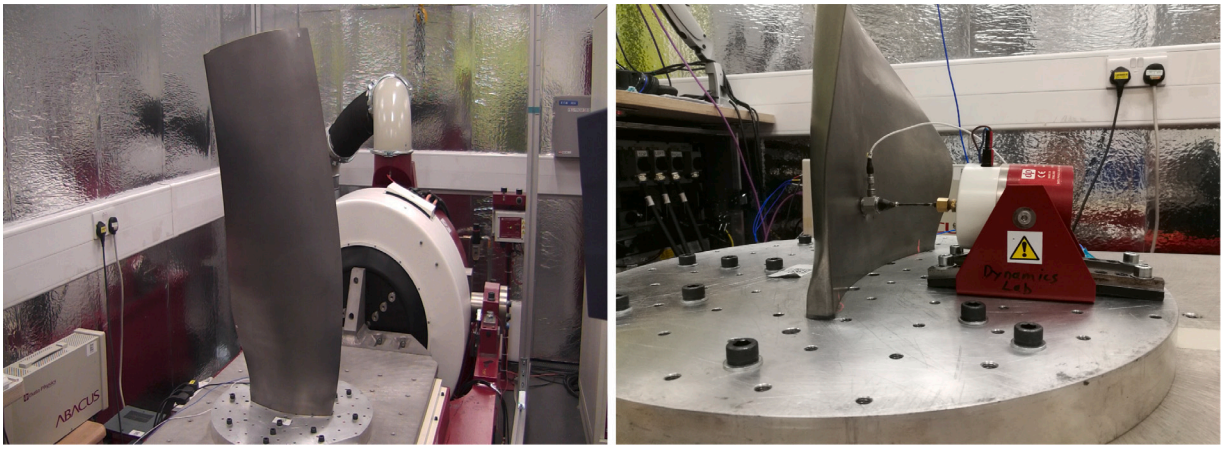

(a) (b)

Fig. 8. Experimental setup [30]: (a) The fan blade (2) The shaker.

5.2. Preliminary data processing

Fig. 10(a) show the first five modes and the tenth mode of the fan blade before the data processing. The first four modes are mainly first bending, second bending, first torsion and edge wide flap dominated. One can also clearly see that there is a clear line in the middle of the fan blade, which distorts the mode shape obtained from 3D SLDV. It is mainly due to the light reflection from the fan blade. Due to this reason, the mode shape of the fifth mode and tenth modes cannot be clearly identified. To reduce the effects of such reflections on the mode shape identification and later data processing, the following filtering was applied. The geometry of the blade was divided into processing blocks along the z-axis. The span of the block was chosen arbitrarily so that the processing would not distort the curvature and twist of the blade. Standard deviation σ, and a mean $\hat{u}$ value was evaluated for each processing block in the x and y direction. The measured relative displacements u that did not satisfy the $\hat{u}_{x,y} - 3 \times \sigma_{u_x,u_y} \leq u_{x,y} \leq \hat{u}_{x,y} + 3 \times \sigma_{u_x,u_y}$ condition for each axis respectively, where considered outliers. In order to remove the reflection line, additionally a radial median filter was applied. Fig. 10(b) shows the post-processed results of the first five modes and the tenth mode. The mode shape of the

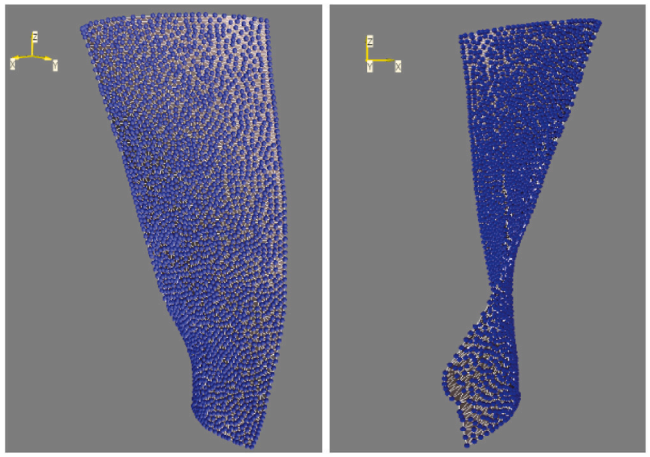

(a) (b)

Fig. 9. A measurement grid of 2016 points [30], where each blue dot represents a scan point: (a) front view and (b) side view from the Polytec Scan Viewer, where x- and y- axes are in the horizontal plane, and the z-axis is vertical.

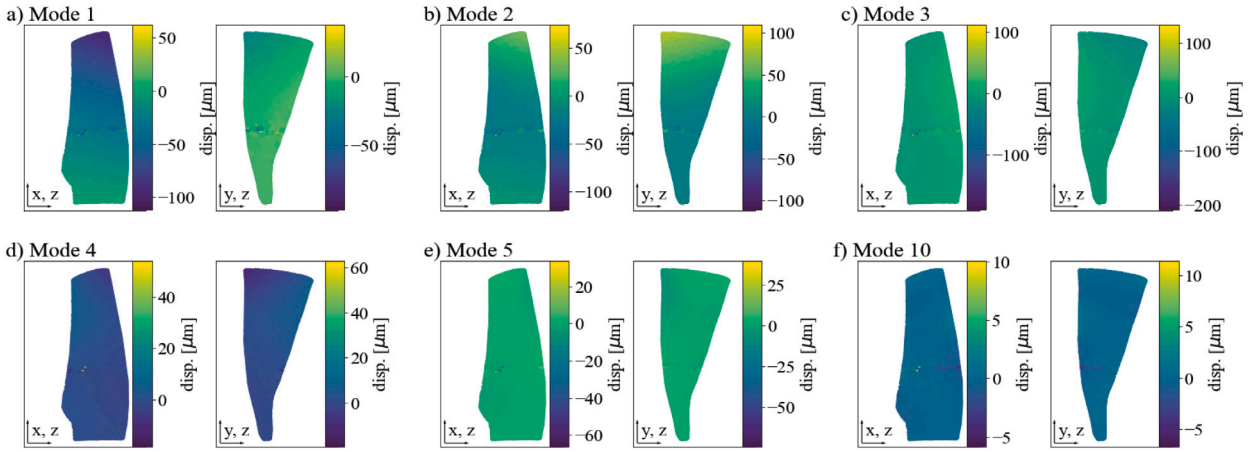

(a) Before prepossessing

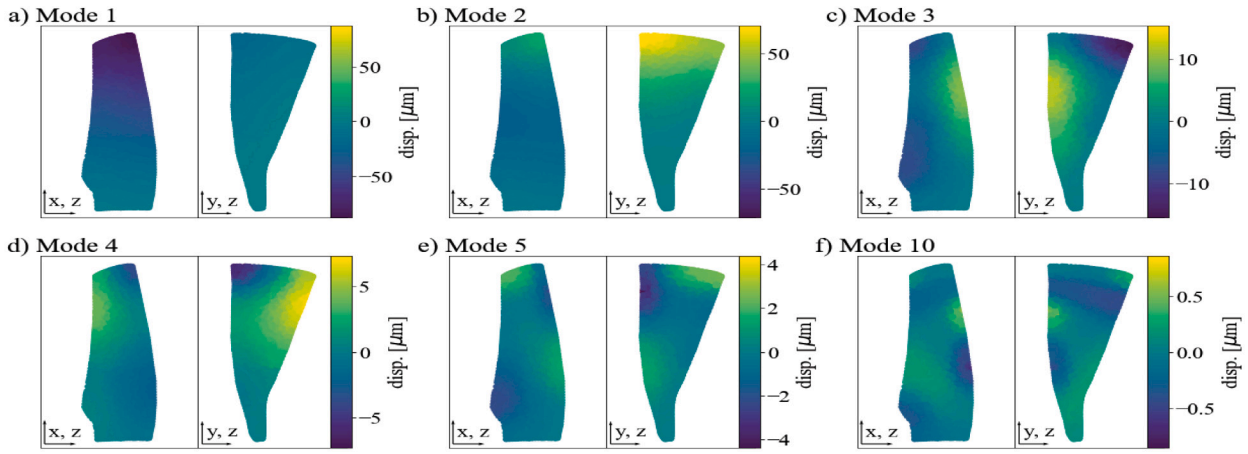

(b) After prepossessing

Fig. 10. Selected modes of the tested fan blade (a) before prepossessing (b) after prepossessing.

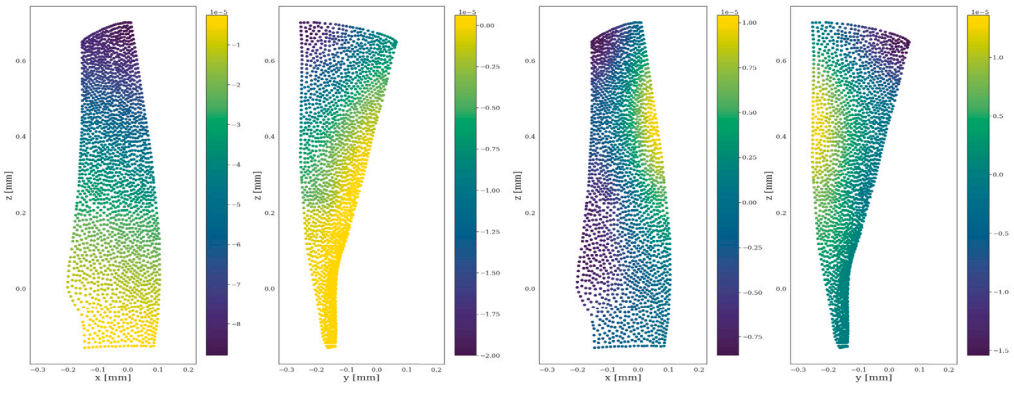

Fig. 11. Example of mode shapes: (a)First mode of the fan blade (b)Third mode of the fan blade.

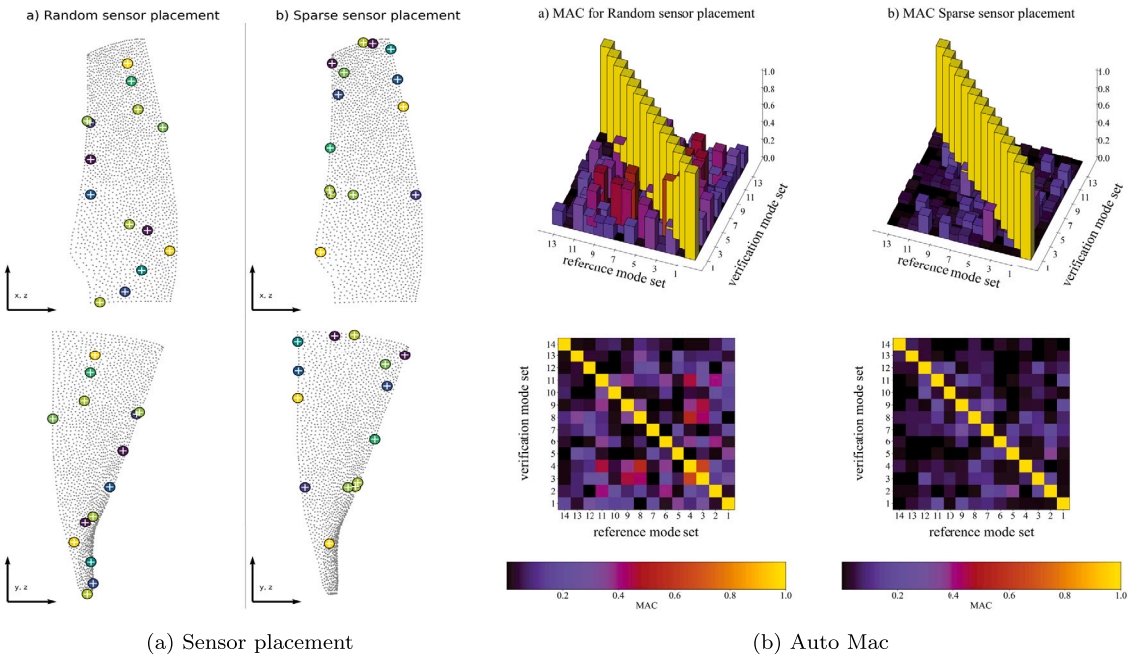

Fig. 12. Comparison of random and optimal sparse sensor placement and Auto Mac values using two sampling methods.

fifth and tenth modes can be better visualized. Figs. 11(a) and 11(b) show the zoomed version of the first and third mode shapes where one can see the reflection line has been removed.

5.3. Auto MAC and response reconstruction

Fig. 12(a) shows the sensor distribution on the fan blade using two different placement methods (a) random sensor placement and (b) optimal sparse sensor placement. In this case, the transform basis to identify the optimal sparse sensor has been obtained from the initial experimental modal analysis in a rapid approach where the numerical model has not been used in this case. Fourteen sensors have been used for the study. It is worth noting that, unlike the random sensor, the locations of optimal sparse sensors obtained through QR factorization with column pivoting are always fixed in the places close to the maximum modal placement at different modes considered. Similarly to the beam example, the greedy matrix QR factorization provides a particularly simple and effective sensor optimization. It is worth noting that the mode shapes obtained from initial modal testing are very noise. Proper orthogonal decomposition is first applied before using QR factorization for optimal sensor placement. Fig. 12(b) shows the Auto MAC values of the first 14 modes for these two sampling methods. One can clearly see that the optimal sparse sensor placement results in much lower off-diagonal values with the same number of sensors. It means the mode shape sampled by the optimal sparse sensor is more

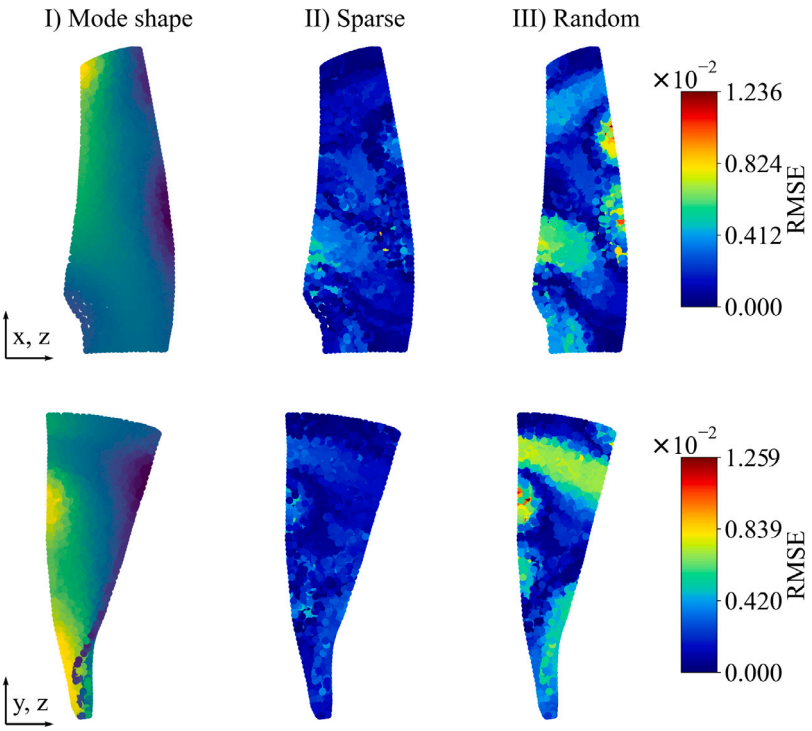

Fig. 13. Comparison of RMSE in response re-construction for the fan blade using ℓ_1 reconstruction.

distinctive than the one sampled by the random sensor approach. For the random sampling method, it can be observed that there is a strong coupling between modes 8, 9, 11 and modes 2, 3, 4.

Figs. 13 and 14 shows the comparison of response construction using these two sampling approaches. Forced frequency response close to mode 10 is tested and studied. The sensor locations are described in Fig. 12(a), and there are 14 sensors used for the reconstruction. Fig. 13 shows the response construction using ℓ_1 algorithm where the first column shows the forced frequency response for the testing, the second column shows the response reconstruction errors using the optimal sparse sensing and the third column shows the response reconstruction errors using random sensing algorithm. One can clearly see that the result from response construction with random sensors leads to much more errors than the sparse method, especially on the edges on both sides where the forced response is very large with the RMSE of 0.75%. With the same number of sensors, the reconstruction errors from optimal sparse sensors are very small, below 0.25% on both sides.

Fig. 14 shows the response construction using ℓ_2 algorithm. Similarly, the first column shows the forced frequency response for testing, the second column shows the response reconstruction errors using the optimal sparse sensing algorithm, and the third column shows the response reconstruction errors using the random sparse algorithm. Similar to ℓ_1 Reconstruction, the performance from optimal sparse sensors is better than random sensors. The response errors with random sensors are much larger than that with ℓ_1 reaching RMSE of 10%. It means that ℓ_1 algorithm is more effective to re-construct the forced frequency response using random sensors. For the optimal sparse sensing approach, the RMSE induced in the ℓ_1 algorithm is around one order smaller than that in the ℓ_2 algorithm.

5.4. Sensitivity analysis

Fig. 15 shows the sensitivity of different numbers of sensors on the accuracy of response construction (RMSE ℓ_1 value) and distinctiveness of the mode shapes (Max off-diagonal Auto MAC value) for the fan blade test case. The red circle represents the results from the random sampling approach, where we have used 50 Monte Carlo simulations. The blue square represents the results from the optimal sparse sensing approach using QR factorization. Please note here, the artificial noise has not been added herein since the measurement from optimal sparse sensing is based on actual testing data. In terms of optimal sparse sensors, the results converge when the number of sensors approaches 12 for Auto MAC value since 14 modes are considered. With further increase of sensor number, the improvement of RMSE and off-diagonal Mac value are very limited. With only four optimal sparse sensors, the response reconstruction can achieve very low RMSE error. In contrast, it requires around 20 random sensors to achieve stable convergence. Even with 20 random sensors, the maximum off-diagonal MAC value can still be very big. Fig. 16 shows the sparsity of the sparse coefficients using random sensor and optimal sensor placement using ℓ_1 algorithm. For this fan blade case with noise

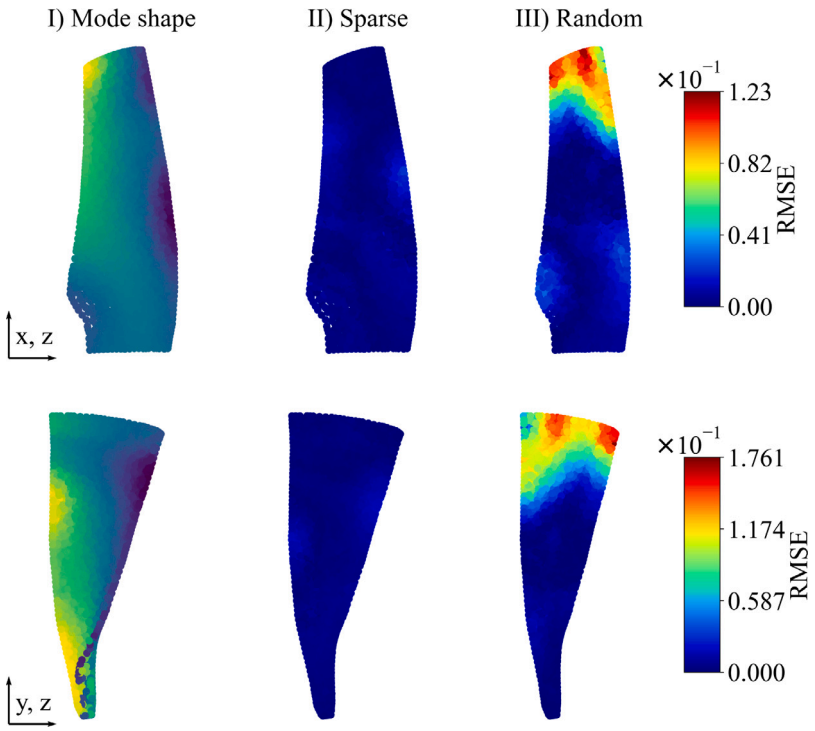

Fig. 14. Comparison of RMSE in response re-construction for the fan blade using ℓ_2 reconstruction.

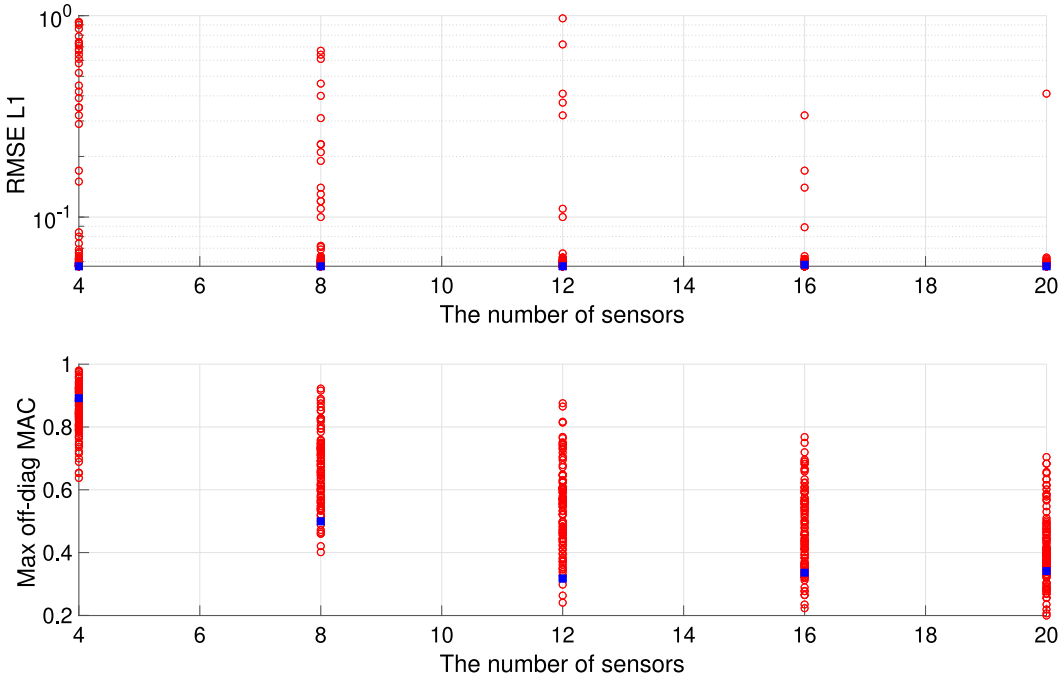

Fig. 15. Sensitivity analysis of fan blade with different sensening approaches.

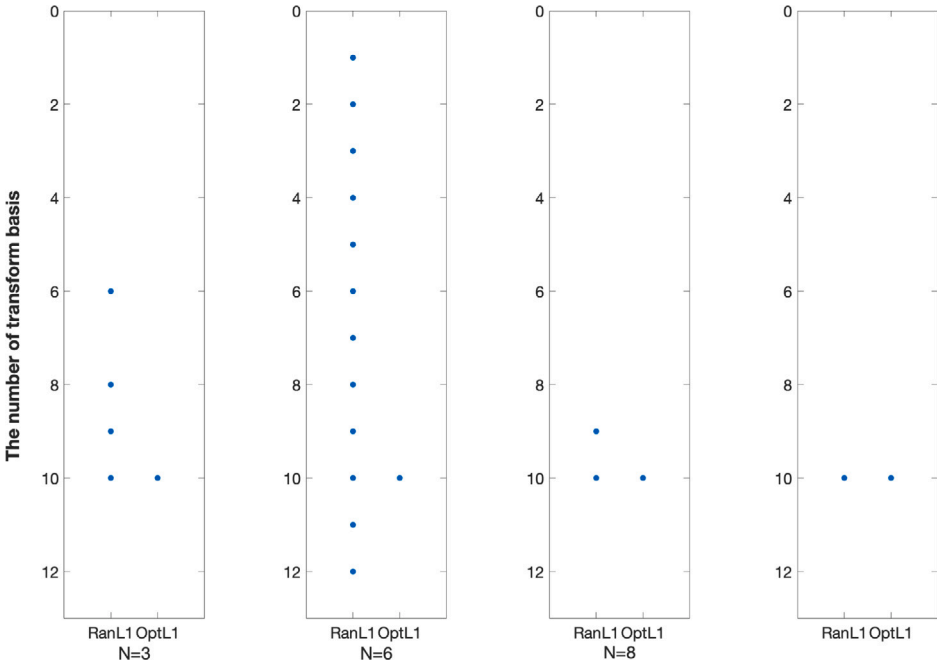

Fig. 16. Comparison of the sparsity of random sensor and optimal sensor approach for fan blade case.

measurement data, it shows that the optimal sensor has shown better sparsity at low number of sensors. With the further increase in the number of sensors, the sparsity of these two approaches converges to a similar level.

6. Conclusions

This paper proposes an efficient optimal sparse sensing technique that significantly reduces the number of scanning points required for accurately reconstructing the dynamical response in full-field experimental modal testing. The optimal sensing locations for measuring points were determined using QR factorization with column pivoting. The basis modes were derived from the vibration data through POD. ℓ_1 algorithm was implemented to promote the sparsity of the limited measurement data and identify the sparse vector for full-field response reconstruction. In this study, ransom sensor placement and the ℓ_2 algorithm are used as the benchmark approaches since they are still widely used in engineering applications. As The performance of auto MAC as a classical criterion to evaluate the performance of the sensor placement are also evaluated between random and optimal sparse sensing approaches.

The methodology was first tested in a cantilever beam with the vibration data obtained from a FE model. It was found that the optimal sparse sensor placement obtains much lower off-diagonal MAC values with the same number of sensors. It indicates the mode shape sampled by the QR method is more statistically distinctive than the one sampled by the random sensor approach. In terms of response reconstruction, no observable difference in response was constructed using the ℓ_1 and ℓ_2 algorithms. However, the response constructed using the sparse approach shows much better agreement with the original response than the random sensor approach especially when the noise is present in the measurement data. The sensitivity study also shows that the sparse sensor approach has a much better convergence in terms of RMSE error and maximum off-diagonal Auto Mac value. The optimal sparse approach is very robust achieving less than 0.005% even when the noise level increases to 10%.

For the second case, a clamped industrial-scale fan blade in aero-engines was considered as a case study. The vibration data was obtained from full-field 3D SLDV vibration testing. A preliminary data processing based on a Gaussian filter was first carried out to remove the reflection line for the first fourteen modes. The optimal sparse sensing locations are identified based the vibration data from initial rapid modal testing. It is highlighted that numerical model has not been used in this case. The results show that the optimal sparse sensor placement results in much lower off-diagonal auto MAC values compared to the same number of random sensors. For the random sampling method, it can be observed that there is a strong coupling between modes 8, 9, 11 and modes 2, 3, 4.

It is also evident that response construction with random sensors leads to much larger errors than the optimal sparse sensors using the QR method, especially in the edges on both sides where the forced response is very large. With the same number of sensors, the reconstruction errors from optimal sparse sensors are three times smaller than those from the random sensing approach. It is shown that the ℓ_1 algorithm shows a much lower RMSE level with respect to response reconstruction than the ℓ_2 algorithm, which is difficult justify the use of ℓ_2 algorithm because of its better convergence. The sensitivity analysis shows that, with only four sparse sensors, the response reconstruction shows a converging RMSE value. In terms of auto MAC value, the results converged when the

number of sensors approached 12. Although this approach is very effective in improving the efficiency of the following testing, the selection of the sensor positions is still dependent on the modal information of the structure either from a validated numerical model or from an initial modal testing. It would be interesting to explore model/experimental free approaches to identify the sensor position in future.

CRediT authorship contribution statement

Jie Yuan: Conceptualization, Formal analysis, Funding acquisition, Methodology, Project administration, Software, Supervision, Writing – original draft, Writing – review & editing. **Michal Szydlowski:** Investigation, Methodology, Writing – original draft, Writing – review & editing. **Xing Wang:** Data curation, Validation, Writing – review & editing, Investigation.

Declaration of competing interest

All authors have participated in (a) conception and design, or analysis and interpretation of the data; (b) drafting the article or revising it critically for important intellectual content; and (c) approval of the final version.

This manuscript has not been submitted to, nor is under review at, another journal or other publishing venue.

The authors have no affiliation with any organization with a direct or indirect financial interest in the subject matter discussed in the manuscript

Data availability

Data will be made available on request.

Acknowledgements

J.Y. would like to acknowledge the Royal Academy of Engineering/Leverhulme Trust Research Fellowship (LTRF2223-19-150). X.W. would like to thank the support from the National Natural Science Foundation of China (Grants 52005522 and 12072378). The authors acknowledge the kind support from Dr. Christoph Schwingshackl at Imperial College London on the experimental testing.

References

[1] G. Toh, J. Park, Review of vibration-based structural health monitoring using deep learning, Appl. Sci. 10 (5) (2020) 1680, http://dx.doi.org/10.3390/app10051680.
[2] D. Ewins, Basics and state-of-the-art of modal testing, Sadhana 45 (2020) http://dx.doi.org/10.1007/BF02703540.
[3] L. Zhu, J. Dai, G. Bai, Sensor placement optimization of vibration test on medium-speed mill, Shock Vib. 2015 (2015) http://dx.doi.org/10.1155/2015/690196.
[4] S. Rothberg, M. Allen, P. Castellini, D. Di Maio, J. Dirckx, D. Ewins, B. Halkon, P. Muyshondt, N. Paone, T. Ryan, H. Steger, E. Tomasini, S. Vanlanduit, J. Vignola, An international review of laser Doppler vibrometry: Making light work of vibration measurement, Opt. Lasers Eng. 99 (2017) 11–22, http://dx.doi.org/10.1016/j.optlaseng.2016.10.023.
[5] J.C. O'Callahan, System equivalent reduction expansion process, in: Proc. of the 7th Inter. Modal Analysis Conf., 1989, 1989.
[6] S.-H. Tsai, H. Ouyang, J.-Y. Chang, Identification of torsional receptances, Mech. Syst. Signal Process. 126 (2019) 116–136, http://dx.doi.org/10.1016/j.ymssp.2019.01.050.
[7] X. Wang, T.L. Hill, S.A. Neild, Frequency response expansion strategy for nonlinear structures, Mech. Syst. Signal Process. 116 (2019) 505–529, http://dx.doi.org/10.1016/j.ymssp.2018.06.027.
[8] C. Touzé, A. Vizzaccaro, O. Thomas, Model order reduction methods for geometrically nonlinear structures: a review of nonlinear techniques, Nonlinear Dynam. 105 (2) (2021) 1141–1190, http://dx.doi.org/10.1007/s11071-021-06693-9.
[9] D.C. Kammer, Sensor placement for on-orbit modal identification and correlation of large space structures, J. Guid. Control Dyn. 14 (2) (1991) 251–259, http://dx.doi.org/10.2514/3.20635.
[10] G.E. Papadopoulos M, Sensor placement methodologies for dynamic testing, AIAA J. 36 (2) (1998) 256–263, http://dx.doi.org/10.2514/2.7509.
[11] D.J. Ewins, Modal Testing: Theory, Practice and Application, John Wiley & Sons, 2009.
[12] Z.L. Tan Y, Computational methodologies for optimal sensor placement in structural health monitoring: A review, Struct. Health Monit. 19 (4) (2020) 1287–1308, http://dx.doi.org/10.1177/1475921719877579.
[13] D. Li, H. Li, C. Fritzen, The connection between effective independence and modal kinetic energy methods for sensor placement, J. Sound Vib. 305 (4–5) (2007) 945–955, http://dx.doi.org/10.1016/j.jsv.2007.05.004.
[14] J. Penny, M. Friswell, S. Garvey, Automatic choice of measurement locations for dynamic testing, AIAA J. 32 (2) (1994) 407–414, http://dx.doi.org/10.2514/3.11998.
[15] R. Semaan, Optimal sensor placement using machine learning, Comput. & Fluids 159 (2017) 167–176, http://dx.doi.org/10.1016/j.compfluid.2017.10.002.
[16] A. Malekloo, E. Ozer, M. AlHamaydeh, M. Girolami, Machine learning and structural health monitoring overview with emerging technology and high-dimensional data source highlights, Struct. Health Monit. 21 (4) (2022) 1906–1955, http://dx.doi.org/10.1177/147592172110368.
[17] S.L. Brunton, J.N. Kutz, Data-Driven Science and Engineering: Machine Learning, Dynamical Systems, and Control, Cambridge University Press, 2019.
[18] Y. Yang, S. Nagarajaiah, Data compression of structural seismic responses via principled independent component analysis, J. Struct. Eng. 140 (7) (2014) 04014032, http://dx.doi.org/10.1061/(ASCE)ST.1943-541X.0000946.
[19] V. Ganesan, T. Das, N. Rahnavard, J.L. Kauffman, Vibration-based monitoring and diagnostics using compressive sensing, J. Sound Vib. 394 (2017) 612–630.
[20] S. Bhowmick, S. Nagarajaiah, Spatiotemporal compressive sensing of full-field Lagrangian continuous displacement response from optical flow of edge: Identification of full-field dynamic modes, Mech. Syst. Signal Process. 164 (2022) 108232, http://dx.doi.org/10.1016/j.jsv.2017.02.002.
[21] Z. Zhang, Y. Xu, J. Yang, X. Li, D. Zhang, A survey of sparse representation: algorithms and applications, IEEE Access 3 (2015) 490–530, http://dx.doi.org/10.1109/ACCESS.2015.2430359, Conference Name: IEEE Access.

[22] Y.C. Eldar, G. Kutyniok, Compressed Sensing: Theory and Applications, Cambridge University Press, 2012.
[23] L. Stanković, E. Sejdić, S. Stanković, M. Daković, I. Orović, A tutorial on sparse signal reconstruction and its applications in signal processing, Circuits Systems Signal Process. 38 (3) (2019) 1206–1263, http://dx.doi.org/10.1007/s00034-018-0909-2.
[24] D. Donoho, Compressed sensing, IEEE Trans. Inform. Theory 52 (4) (2006) 1289–1306, http://dx.doi.org/10.1109/TIT.2006.871582, Conference Name: IEEE Transactions on Information Theory.
[25] E.J. Candes, M.B. Wakin, An introduction to compressive sampling, IEEE Signal Process. Mag. 25 (2) (2008) 21–30, http://dx.doi.org/10.1109/MSP.2007.914731, Conference Name: IEEE Signal Processing Magazine.
[26] V. Roth, The generalized LASSO, IEEE Trans. Neural Netw. 15 (1) (2004) 16–28, http://dx.doi.org/10.1109/TNN.2003.809398.
[27] T.T. Do, L. Gan, N. Nguyen, T.D. Tran, Sparsity adaptive matching pursuit algorithm for practical compressed sensing, in: 2008 42nd Asilomar Conference on Signals, Systems and Computers, 2008, pp. 581–587, http://dx.doi.org/10.1109/ACSSC.2008.5074472.
[28] S. Mallat, Z. Zhang, Matching pursuits with time-frequency dictionaries, IEEE Trans. Signal Process. 41 (1993) 3397–3415, http://dx.doi.org/10.1109/78.258082.
[29] S. Boyd, L. Vandenberghe, Convex Optimization, Cambridge University Press, 2004.
[30] X. Wang, M. Szydlowski, J. Yuan, C. Schwingshackl, A Multi-step Interpolated-FFT procedure for full-field nonlinear modal testing of turbomachinery components, 169, 2022, 108771, http://dx.doi.org/10.1016/j.ymssp.2021.108771,
[31] A.A. Ozdemir, S. Gumussoy, Transfer function estimation in system identification toolbox via vector fitting, IFAC-PapersOnLine 50 (1) (2017) 6232–6237, http://dx.doi.org/10.1016/j.ifacol.2017.08.1026.